

Special Issue: Future of Cell Biology

## Review

# Intravital Correlative Microscopy: Imaging Life at the Nanoscale

Matthia A. Karreman,<sup>1</sup> Vincent Hyenne,<sup>2,3,4,5</sup>  
Yannick Schwab,<sup>1,\*</sup> and Jacky G. Goetz<sup>2,3,4,5,\*</sup>

**Studying key biological events within complex model systems relies on dynamic and functional imaging at optimum spatial and temporal resolutions. Intravital correlative light and electron microscopy (intravital CLEM) combines imaging living multicellular model systems with electron microscopy, and offers full ultrastructural details of dynamic or transient events *in vivo*. However, routine use of intravital CLEM is hindered by multiple technological challenges faced when targeting a micron-size object (e.g., single cells or organelles) in a complex living organism. Recently, various approaches have been developed to overcome these limitations. In this review we outline the current methods and present the power of intravital CLEM in different fields of research. Finally, we describe approaches that will make intravital CLEM a routine, quantitative method for high-resolution cell biology *in vivo*.**

## Intravital CLEM for Correlating Structure to Function *In Vivo*

While *in vitro* models offer multiple advantages for cell biology, they fail to fully recapitulate the complexity of tissues *in vivo*. To achieve a complete understanding of biological processes, these are therefore best studied in living animals. Many functional techniques can be employed for understanding a specific phenomenon *in vivo*, among which is intravital microscopy (IVM). IVM allows visualization of dynamic and specific events in living animal model systems, at optimal temporal resolution and, if required, over long periods of time [1–4] (Box 1). This can be done using organelle- or protein-specific fluorescent tags, or using functional probes, both of which inform on the location and on the function of the event of interest. Electron microscopy (EM), by contrast, is the only method so far to reveal the rich subcellular landscape at high resolution. Because EM also resolves the ultrastructural context, cellular interactions with their surrounding microenvironment can be studied in tissues.

Correlative light and electron microscopy (CLEM) combines the advantages of both imaging modalities, allowing the targeting of the event or the specific molecule of interest in space and time using light microscopy, and subsequently imaging the exact same area in the specimen at high resolution with EM. CLEM has yielded seminal results *in vitro*, either on cultured cells or on organotypic tissue-slices [5–9]. This success has led to the design of numerous strategies to correlate dynamic fluorescence microscopy (FM) to EM [10–16]. In an intact organism, correlating IVM to EM using intravital CLEM enables high temporal and spatial resolution studies of crucial biological events as they take place in their native environment. IVM allows the monitoring of behavior over time, or the assessment of function, provided that functional probes such as *in vivo* sensors are available. Next, EM permits studying the object, and its direct surroundings, at high resolution.

### Trends

Modern imaging for life sciences is performed on model organisms. It aims at integrating functional information obtained *in vivo* with high spatial resolution.

Intravital CLEM uniquely enables the visualization of key biological events in living multicellular organisms and at high resolution.

Bimodal probes are specifically developed to mark the event of interest for *in vivo* and EM imaging.

Automating correlative workflows to enable higher throughput is a prerequisite for routine and quantitative applications.

<sup>1</sup>Cell Biology and Biophysics Unit, European Molecular Biology Laboratory (EMBL), Heidelberg, 69117 Germany

<sup>2</sup>Microenvironmental Niche in Tumorigenesis and Targeted Therapy (MN3T), Institut National de la Santé et de la Recherche Médicale (INSERM) Unité 1109, 67200 Strasbourg, France

<sup>3</sup>Université de Strasbourg, 67000 Strasbourg, France

<sup>4</sup>LabEx Medalis, Université de Strasbourg, 67000 Strasbourg, France

<sup>5</sup>Fédération de Médecine Translationnelle de Strasbourg (FMTS), Université de Strasbourg, 67000 Strasbourg, France

\*Correspondence: [schwab@embl.de](mailto:schwab@embl.de) (Y. Schwab) and [jacky.goetz@inserm.fr](mailto:jacky.goetz@inserm.fr) (J.G. Goetz).

### Box 1. Intravital Microscopy: Watching Cells in their Natural Habitat

Because it allows cellular behavior to be observed in its native context, IVM is instrumental in acquiring new knowledge in the cell biology of developmental, physiological, and pathophysiological processes. Uniquely, *in vivo* models integrate the complex cellular heterogeneity, the mechanical and topological properties of the tissues, the presence of soluble factors, as well as optimal blood perfusion. Intravital imaging can be easily performed on naturally transparent organisms such as embryos or larvae, and this has been particularly useful for studies in *Drosophila*, *C.elegans*, zebrafish, and the chick embryo (Figure 1A). Because these models are suited for non-invasive confocal microscopy, they can also be adapted to model diseases such as cancer [100,101]. Light-sheet microscopy, which is less phototoxic than confocal and multiphoton microscopy, provides access to long-term volume imaging of fragile samples (early mouse embryos) [86]. It is also possible to image a complete living organism, provided that they are translucent [87,102].

Non-invasive IVM in mouse models is rare, mostly because of light absorption that occurs when trying to reach cellular events localized deep in the tissue. Intact tissues such as the epidermis or the subcutaneous layers (~100  $\mu\text{m}$ ) can be reached using two-photon excitation microscopy (2PM) [36,49,103,104]. However, most internal organs either need to be surgically exposed to 2PM imaging or to be reached by endo-microscopy (Figure 1B). Via surgical exposure, 2PM has been successfully used to image organs such as the tongue, the leg muscles, the dermis, and organs of the gastrointestinal tract. Because these approaches are invasive and not compatible with longitudinal recordings of the animals, scientists have developed imaging windows that provide deep access (up to few hundred  $\mu\text{m}$ ) to brain [71], lung [105], mammary tissue [1], abdominal organs [106], and subcutaneous tissues [107]. Virtually any biological event can be studied with IVM, but imaging windows have been so far widely designed and used for tracking different steps of tumor progression [68]. An alternative to surgical exposure is the use of micro-endoscopic tools that are less invasive and still provide access to important organs such as the brain, heart, airways, and colon [108]. In this case the micro-endoscope is inserted through natural orifices or via small surgical openings. It must be noted that this approach is of lower resolution and has a smaller field of view compared to confocal FM and 2PM.

Another advantage of the 2PM, in addition to its penetration depth, is the visualization of non-labeled structures by non-linear fluorescence imaging. Non-centrosymmetric molecules, such as myosin (muscle) and collagen, are imaged using second harmonic generation [109]; interfaces between water and lipids or proteins (e.g., cellular membranes) can be visualized with third harmonic generation [110]; and lipids can be analyzed using CARS (coherent anti-Stokes Raman scattering) [111]. A recent review on intravital imaging provides a comprehensive table listing the different *in vivo* imaging techniques and their applications [112].

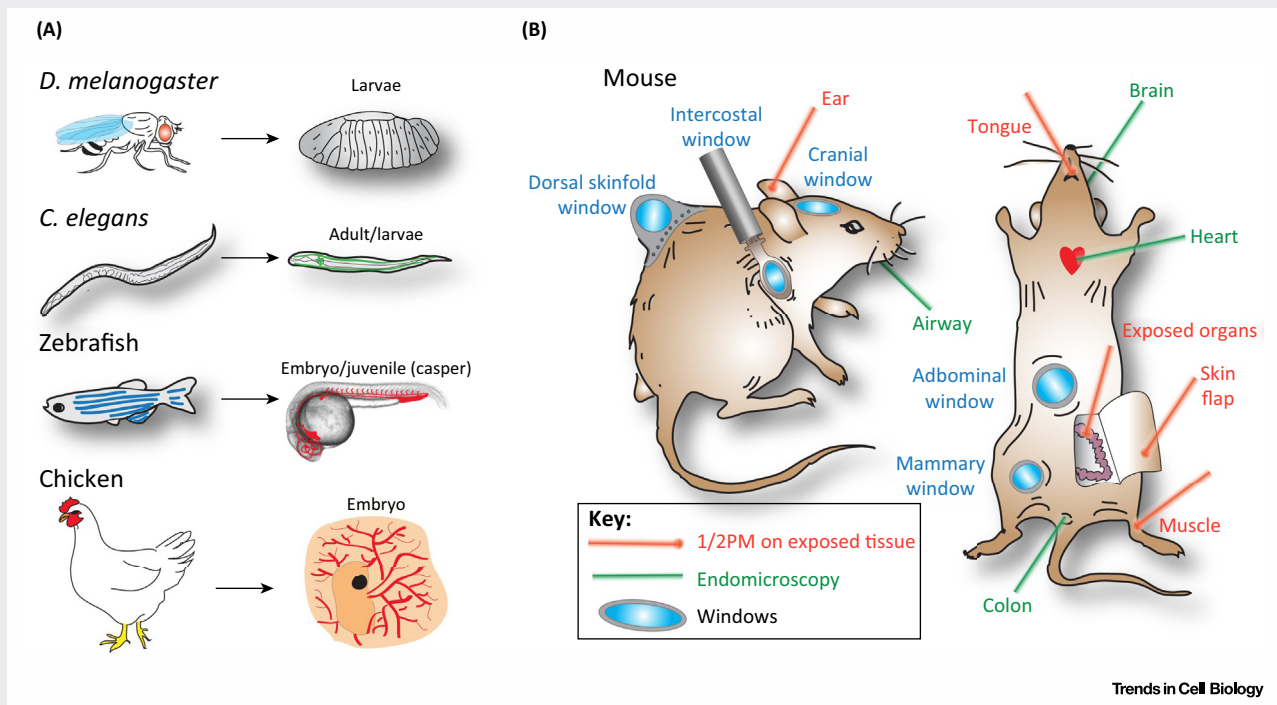
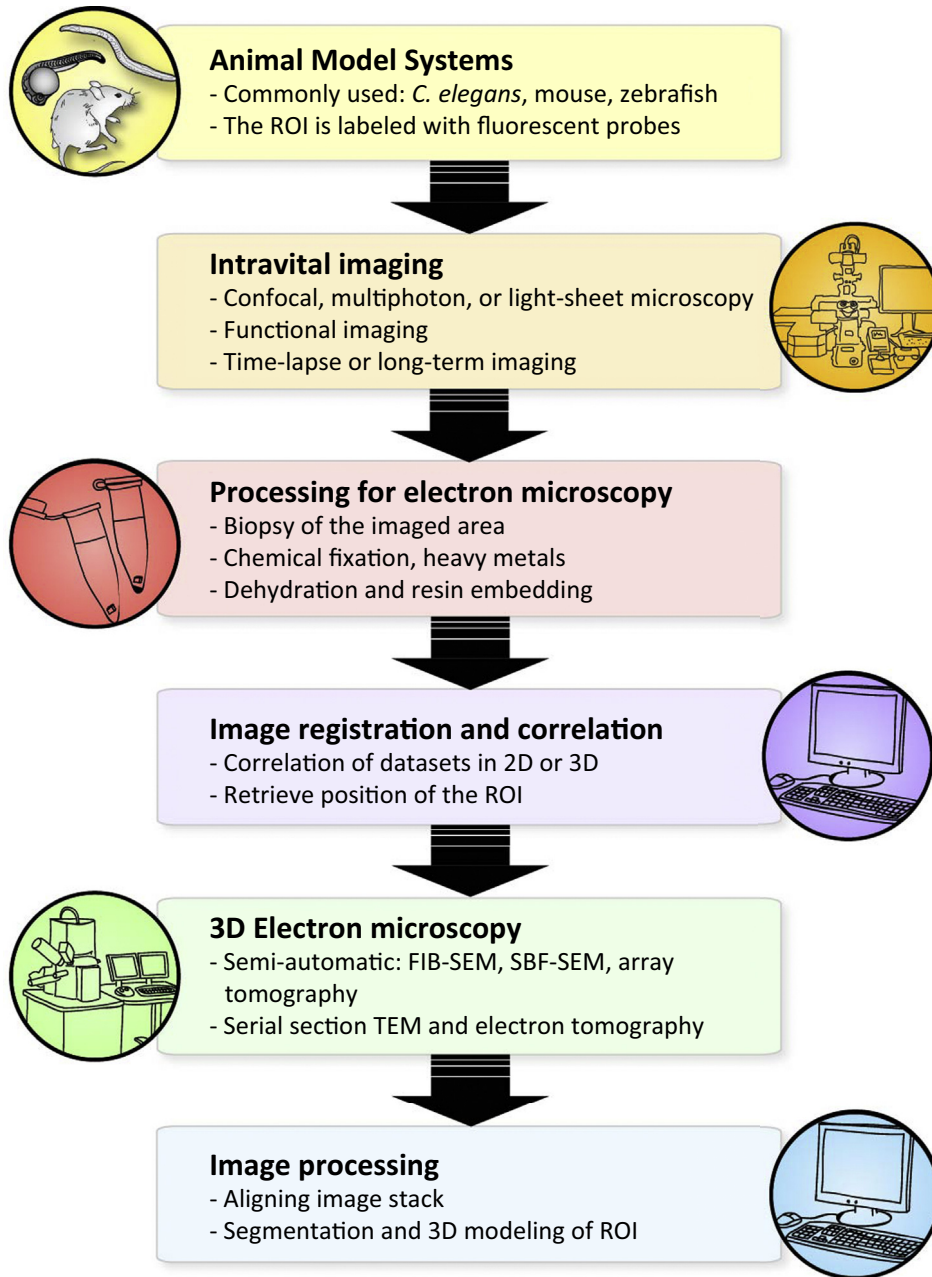


**Figure 1. Model organisms used in intravital correlative microscopy.** (A) *in vivo* microscopy can be easily applied to transparent organisms. (B) In bigger opaque animals, such as the mouse, some thin tissues can be directly observed by multiphoton microscopy, while others need to be surgically exposed. Alternatively, imaging windows can be surgically implemented on the animal or specific tissues can be reached by endo-microscopy.

In this review we focus on the combination of *in vivo* microscopy on animals and EM, which we refer to as 'intravital CLEM'. Our aim is to facilitate and promote intravital CLEM by offering an overview of the existing workflows (Figure 1, Key Figure), as well as by illustrating some of their applications to various model-systems. We discuss the potential and limitations of each

## Key Figure

## Outline of an Intravital Correlative Light and Electron Microscopy (CLEM) Workflow



Trends in Cell Biology

**Figure 1.** Different animal models can be genetically engineered and observed *in vivo*, allowing dynamic and functional imaging of any biological event of interest. After fixation and processing for EM, the position of the region of interest (ROI) within the resin block can be retrieved by correlating the volume acquired by intravital imaging and the fixed tissue. It allows 3D electron microscopy acquisition and segmentation of the ROI.

### Box 2. Sample Preparation for EM

Classical EM processing involves chemical fixation, infiltration with heavy metals, dehydration, and resin embedding. This procedure generates a sample that is comparatively stable in the vacuum of the electron microscope, and is suitable for sectioning and EM imaging. Chemical fixation is a slow process and prone to introduce structural artifacts, whereas high-pressure freezing (HPF) stops processes in a few milliseconds and yields better ultrastructural preservation [29,113]. The advantages of HPF were exploited in the study of small organisms, where the event of interest can be monitored by IVM, followed by rapid cryo-fixation [17,31]. Subsequently, the sample can be freeze-substituted and embedded in resin [114], or the sample can be imaged under cryo-conditions with EM [115]. Interestingly, the use of cryo-FIB-SEM to generate thin lamellas has recently been introduced to perform cryo-TEM tomography on multicellular specimens [116]. Such techniques not only enable ultrastructural analysis of samples in a close to native state but can also reveal the structure of macromolecular complexes at near-atomic resolution. The application of such approaches in intravital CLEM on small model organisms is to be expected in the near future.

Nevertheless, efficient vitrification of biological specimens by cryo-fixation is limited to a maximum of 200  $\mu\text{m}$  (when using HPF) or even less, for example for challenging tissues such as mouse brain (10–20  $\mu\text{m}$ ) [113]. Cryo-fixation of a region from large specimens would require dissection, which unavoidably leads to profound artifacts. Therefore, chemical fixation is often the only alternative to efficiently immobilize large tissue samples in an intravital CLEM workflow. Following initial fixation, heavy metals are added to the tissues, such as osmium tetroxide or uranyl acetate. In addition to being strong fixatives, heavy metals are also contrasting agents for EM that allow the visualization of subcellular structures such as endo-membranes, the cytoskeleton, and protein complexes. Moreover, heavy metal staining is of prime importance when imaging large volumes by automated serial imaging methods using scanning EM (Box 3 and Figure 1 in main text), which are highly suited to imaging multicellular specimens.

technique, and we introduce emerging approaches that will further push the efficiency and throughput of intravital CLEM.

### Keeping the Region of Interest (ROI) in Sight: Approaches for Intravital CLEM

Although imaging subcellular regions in multicellular organisms by FM can be done on large volumes (Box 1), EM imaging demands a reduction in sample size and specialized tissue fixation and processing steps (Box 2). These processing steps have a dramatic impact on the ability to correlate EM to the IVM dataset (Boxes 2 and 3). Moreover, EM processing results in modifications to the dimensions and orientation of the sample, making it impossible to accurately track the position of the ROI inside the resin block.

The most crucial step is the retrieval of the object imaged *in vivo* from the EM-processed 3D sample. In the case of nematode embryos [17,18] and small model organisms [19,20], the entire

### Box 3. Bimodal Probes for Intravital CLEM

The ideal probe for performing intravital CLEM is specific, biocompatible, and, importantly, visible both in LM and EM. Several attempts have been made to develop such bimodal probes, the most potent of which involves genetically encoded fluorescent molecules, combined with a system able to generate electron-dense deposits. The genetically encoded miniSOG is a fluorescent protein that, upon blue light illumination, generates oxygen singlets that in turn induce local DAB photo-oxidation. The result is the accumulation of a highly osmiophilic, thus electron-dense, deposit visible by EM [117]. However, its reduced brightness and the requirement for light to induce DAB photo-oxidation precludes its use in thick volumes of tissues because of light scattering. Alternatives are emerging, such as the fusion of a fluorescent protein with a genetically encoded peroxidase (e.g., Flipper [118]). While this combination offers the best probes in each imaging mode, it results in a large fusion protein (most fluorescent proteins and peroxidases are around 25 kDa) and therefore requires functional validation before being used in an intravital setting. In an alternative approach, peroxidase has been fused to a GFP-binding protein and coexpressed with the GFP-tagged protein of interest in a living animal [119]. This modular system relies on the potent APEX2 peroxidase [120], and allows fast and precise subcellular localization of various proteins. The recently developed click-EM technology offers an interesting alternative to fluorescent proteins because it allows non-protein biomolecules to be metabolically labeled with single-oxygen generating dyes using 'click-chemistry' ligations [121].

Other probes specifically designed for *in vitro* CLEM (such as the FlAsH/ReAsH system, [122]), as well as small organic or inorganic affinity-based molecules (e.g., quantum dots), may presently be restricted to specific cases of IVM [123]. It remains problematic that some of these probes are not biocompatible or may even be toxic, and it is challenging to deliver these probes to the cells in a living organism.

sample can be screened with EM to retrieve the ROI. Serial imaging of full samples from larger organisms, however, is highly cumbersome and results in unnecessarily large datasets. We outline here methodologies that keep track of the ROI when moving from IVM to EM, either by relying on bimodal probes (Box 3) or on anatomical or artificially introduced landmarks that are visible in different imaging modalities.

#### Translating Staining for *In Vivo* Imaging to EM

Intravital CLEM approaches have elaborated on existing methods for *in vivo* microscopy. These rely on genetically encoded fluorescent proteins to study, in living animals, the expression and localization patterns of specific proteins, and to analyze the fate and behavior of specific cells or subcellular compartments. While these can be easily observed in transparent or relatively thin embryos using conventional fluorescence techniques, in two-photon excitation microscopy (2PM), the use of fluorophores excitable in the near infrared spectrum allows deeper observation in somewhat opaque tissues because the light is less absorbed and scattered at these wavelengths (700–900 nm, Box 1). However, only a few studies have translated the fluorescent signal recorded with intravital imaging to EM [21–24]. This has been achieved either by preserving the fluorescence of the object of interest while processing for EM or by converting it to an electron-dense material visible by EM, mostly through DAB (3,3'-diaminobenzidine) oxidation [13,25,26]. Oxidation of DAB into an osmiophilic product can be achieved either by using peroxidase-coupled antibodies [21], photo-oxidation by a fluorochrome or a fluorescent protein [22,24], or by using genetically encoded peroxidases [23]. Fluorescence can be preserved in the resin block through chemical fixation using low amounts of heavy metals [27,28] or through high-pressure freezing (HPF) followed by freeze substitution and lowicryl embedding [29,30]. The latter constitutes a promising solution to follow the same staining in both imaging modes (Box 3), with great potential for intravital CLEM.

#### Correlating *In Vivo* Microscopy to EM Based on Landmarks

Limiting 3D electron microscopy (3DEM) imaging (Box 4) to the area that was identified with IVM is one of the most effective approaches for intravital CLEM. This approach requires precise identification of the position of the ROI within the processed sample, even when fluorescence is abolished (Box 2). Targeted ultramicrotomy relies on overlaying 2D IVM images on a macroscopic image of the resin-embedded sample, for example *C. elegans*, zebrafish, or *Drosophila* embryos (Figure 2A and Box 1). The superimposed IVM image provides the position of the ROI, and this location can then be carved onto the resin block using a laser dissection microscope [31,32] (Figure 2A). The markings are subsequently used as a guide to target the ROI using ultramicrotomy. Although highly effective in comparatively flat samples such as the nematode or the zebrafish embryo, this method is limited to retrieving the *x* and *y* coordinates of the ROI and it does not reveal its *z* position within the block. For large 3D samples, alternative approaches are thus required.

One effective approach is to map the position of the ROI with respect to landmarks in the tissue surrounding the ROI (Figure 2A). Endogenous or artificially introduced landmarks are used as a guide to retrace the position of the ROI following EM processing. Tissue features can be effectively used as landmarks provided that they are recognizable both with IVM and during the subsequent processing and imaging procedures. The vascular network can be imaged *in vivo*, for example by using transgenic animals in which endothelial cells stably express fluorescent proteins, or by injecting fluorescent dyes into the circulation. Alternatively, fluorescent red blood cells can be injected to reveal vessel perfusion *in vivo* [33]. In thin and largely transparent tissues [34,35], vessels are still recognizable after resin embedding and can be used to select the area to be imaged with EM. In mouse skin tissue, networks of vessels and collagen fibers were exploited to correlate the IVM dataset to LM images of thick 500 nm sections that were obtained while progressing through the ROI [36]. In zebrafish, trimming and

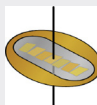
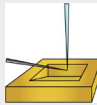
## Box 4. Volume EM: Automating Subcellular Imaging in 3D

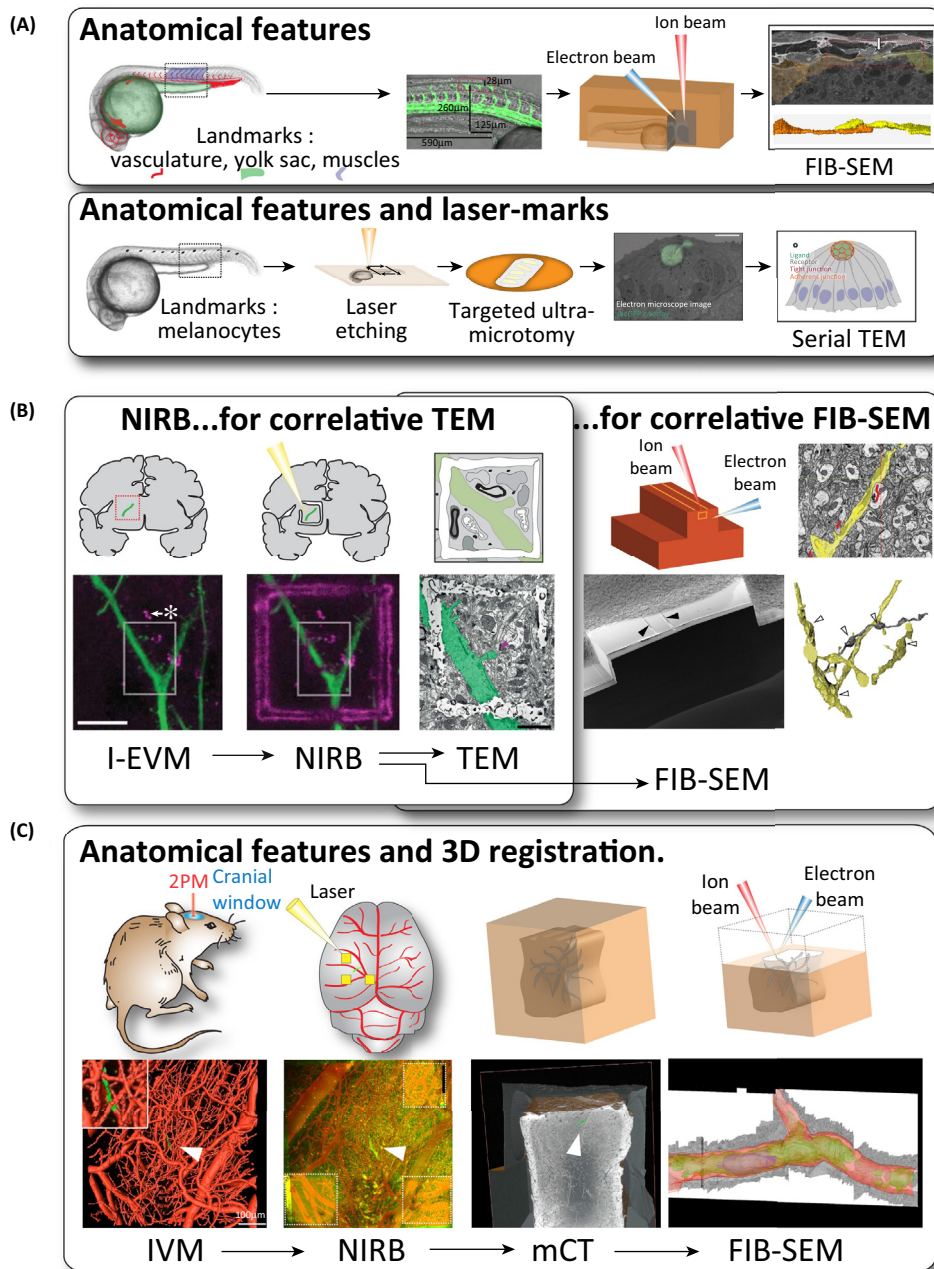
Recent technological advances have resulted in the development of 3D electron microscopy (3DEM) to image voluminous samples ranging from whole cells to organisms. 3DEM imaging has mostly been performed by serial-section transmission EM [124,125], which can be combined with serial electron tomography (Table I). Scanning TEM (STEM) tomography allows thicker sections (0.5–1  $\mu\text{m}$ ) to be imaged, thus permitting larger volumes to be visualized [126,127]. However, serial sectioning is cumbersome, results in an inevitable loss of material, and sections are deformed by the cutting process. Moreover, the sectioning, staining, and imaging steps demand constant input from the operator. Scanning EM (SEM), which was traditionally used in life sciences to obtain topographic images of samples, is now emerging as the future of 3DEM (Table I).

SEM offers semi-automatic approaches for 3DEM. Large sequences of serial sections, mounted on a solid substrate, can be imaged with SEM [63,128–132]. Coined as ‘array tomography’, this method involves performing repetitive immunofluorescent labeling, FM, and EM imaging of serial thin sections mounted on glass slides [133–136]. Adjustments to the method have been made to improve SEM imaging conditions [137,138]. Collecting serial sections has been automated by the invention of the automated tape collection ultramicrotome (ATUM) [139–141]. In this technique serial sections are collected on a tape as they come off the knife. The tape is split into numerous fragments that are mounted on large wafers, which are imaged. Importantly, the acquisition step is automated by the development of microscope-controlling software that recognizes and images the sections (e.g., [141] and Atlas 5, Zeiss).

Alternative approaches have been developed to image the block-face of the sample following removal of thin layers of biological material. Arguably, the block-face suffers less from deformation compared to thin sections, and imaging with SEM is limited to the first ~5–60 nm of the sample surface. Repetitive cycles of sectioning and SEM imaging of the block-face enable 3D image stacks of the sample to be generated [63,128,130,131,142]. This can be achieved in two ways: (i) focused ion beam FIB-SEM combines a SEM column, for imaging, with an FIB column, that sputters thin layers (down to 3 nm) of biological material [142]. (ii) Using serial block-face SBF-SEM [143,144], 30–100 nm sections of the sample are removed by a custom-built microtome mounted inside the SEM chamber. In both FIB-SEM and SBF-SEM, sectioning–imaging cycles are performed automatically and may run over several hours or days, depending on the desired image volume and voxel size. These techniques now enable visualization of the ultrastructure of samples of large dimensions, revealing complex organelle networks in cells, or enabling the analysis of cell–cell contacts in large tissues.

Table I. Approaches for 3D Electron Microscopy

3DEM Approach	Typical Lateral Resolution (xy)	Typical Axial Resolution (z)	Sample Volume	Manual parts of Procedure	Notes	Selected Reviews
 Serial section TEM	1–5 nm	50–100 nm	Block-face: 0.5 mm $\times$ 0.3 mm	Trimming block, serial sectioning, TEM imaging	May be combined with serial electron tomography, improving the resolution in z to > 1 nm. Multiple acquisitions are possible, and sections are preserved.	[63,125, 128,130, 131]
 Array tomography (with ATUM) SEM	4–8 nm	40–200 nm	Block-face: > 0.5 mm $\times$ > 0.3 mm	Trimming, serial sectioning (unless performed with ATUM), monitoring microscope	Multiple acquisitions are possible, sections are preserved. May be combined with immunolabeling and FM/LM.	[63, 128–132]
 Focused ion beam SEM	4–8 nm	4–8 nm	Size of the stub: mm range. The imaged volume is smaller (50 $\times$ 50 $\times$ 50 $\mu\text{m}^3$ )	Trimming and mounting sample, setting up and monitoring microscope	Material is ablated and thus lost. The block-face is imaged: less deformation, resulting in improved post-acquisition alignment. FIB can be used for imaging.	[63,128, 130,131, 142]
 Serial block-face SEM	5–8 nm	100 nm	300–500 $\mu\text{m}$ in xy, 200–500 $\mu\text{m}$ in height. Imaged volume may be the full block-face or selected ROIs	Trimming and mounting sample, setting up and monitoring microscope	Sections are not preserved. The block-face is imaged: less deformation, resulting in improved post-acquisition alignment.	[63,128, 130]



## Trends in Cell Biology

**Figure 2. Approaches Used To Retrieve the ROI Observed by Intravital Microscopy (IVM) in the Resin Block.** (A) Anatomical features (e.g., melanocytes, vasculature, yolk sac, muscles) present in the tissue can be used to locate the ROI (region of interest) by focused ion-beam scanning EM (FIB-SEM) [37], or post-embedding laser etching can enable targeting for serial transmission electron microscopy (TEM) [32]. (B) The ROI can be delimited in x-y by near-infrared branding (NIRB) of the living tissue following intravital imaging which enables precise EM acquisition by TEM or by FIB-SEM [47,48,55]. (C) 3D registration of the anatomical features present in the tissue (such as blood vasculature), visible in IVM and microCT (mCT), allows the ROI to be precisely targeted in 3D and volume ultrastructure to be acquired by FIB-SEM [49].

approaching the ROI can be monitored by relying on structural features such as the yolk sac, notochord, melanocytes, muscles, endothelial cells, and blood vessels [32,36–40] (Figure 2A).

#### Retrieval of the ROI within Vibratome Sections: From LM to Near-Infrared Branding

For voluminous specimens such as the mouse brain, the ROI can be retrieved by screening serial thick (60–100  $\mu\text{m}$ ) vibratome sections of the tissue. Inspecting these sections by LM allows quick retrieval of the area imaged *in vivo*. The ROI can be marked by photo-oxidation of fluorophores or by affinity labeling with peroxidases (Box 3). These deposits are visible in the vibratome sections before [22,23,41] and after resin-embedding [25]. DAB-labeling of GFP-expressing neurons has been used in mouse brain [21,24,42–45], based on an *in vitro* CLEM approach using cultured brain slices [46]. In this technique, IVM through a cranial window (Box 1) is followed by perfusion fixation, and 60  $\mu\text{m}$  vibratome sections of the brain are produced parallel to the imaging plane. Repetitive freeze–thaw cycles of the cryo-protected brain slices ensures effective affinity-labeling of the GFP-expressing neurons and subsequent targeting with peroxidases, which in turn generates DAB deposits. Following resin embedding, the position of the ROI is retrieved in the brain slice based on correlating the visible vascular patterns with the IVM dataset. Following serial sectioning of the area of interest, the DAB-labeled neuron is retrieved while screening the sections with transmission electron microscopy (TEM).

Alternatively, near-infrared branding (NIRB) can be used to mark the position of the ROI in the vibratome section (Figure 2B) [47]. Following IVM and chemical fixation, the vibratome sections are screened to retrieve the fluorescent ROI. Physical markings are created by NIRB, consisting of tissue damage induced by a high-powered slow-scanning laser in the same z plane or above the ROI [47]. These marks are visible in the tissue section by imaging at a low magnification (macroscopy) and by EM, facilitating retrieval of the ROI during processing and EM imaging. Light scattering induced by the tissue limits the depth of the branding, and NIRB is therefore mostly performed to mark the surface of the sample [36] or the inside of the vibratome sections [47,48]. The technique has been proven effective in various tissue types, including mouse brain [47–49], spinal cord [47], and skin [36,49].

A correlative IVM and focused ion-beam scanning EM (FIB-SEM, Box 4) workflow was developed to retrieve single neurons in brain tissue, and is now routinely used in many studies [48,50–54] (Figure 2B). In this technique, IVM of GFP-expressing neurites is followed by perfusion fixation and vibratome sectioning of the mouse brain. The pattern of blood vessels observed *in vivo* is used to retrieve the ROI within the vibratome sections, by image registration, and this area is subsequently marked by NIRB. Following resin embedding, these NIRB marks are visible and are copied to the resin surface by laser etching. These supplementary landmarks, as previously used for targeted ultramicrotomy [31,38], greatly facilitate the trimming of the resin block to expose the sample for volume EM imaging [55] (Figure 2B).

#### MicroCT to Target the ROI inside an EM-processed Sample

Screening serial resin-sections or vibratome-sections of the sample enables the retrieval of the ROI in *x*, *y*, and, importantly, in *z*. For obvious reasons, such as time constraints, browsing through the sample using 50–500 nm serial sections is limited to small organisms or flat tissues. Retrieving the ROI inside vibratome-sections requires the targeted structure to be much smaller than the thickness of the section. In the case of dendritic spines, boutons, axons, and synapses [48,50–54,56], the features are sufficiently small to be captured in full inside a 60–100  $\mu\text{m}$  vibratome section. However, in studies of metastatic events, full 50–80  $\mu\text{m}$  sized tumor cells were targeted in living mice [49]. In this case it was necessary to avoid disrupting the integrity of the cell of interest that could occur when obtaining vibratome sections. Therefore, an alternative approach was developed that bypasses serial vibratome sections and screening of the tissue. First, the *xy* position of the imaged volume is marked at the tissue surface using NIRB [36,47],



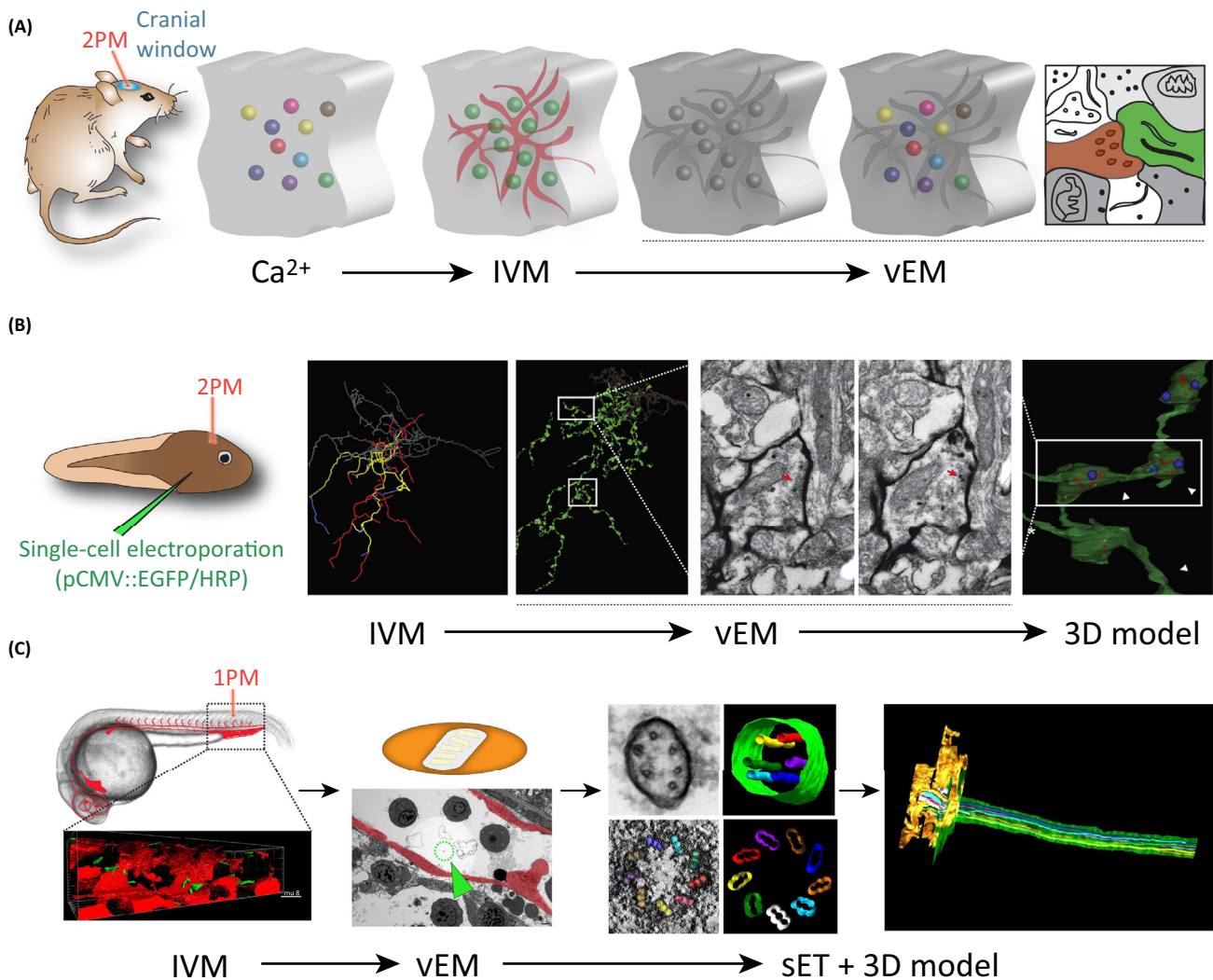
enabling the excision of a  $> 1 \text{ mm}^3$  biopsy containing the ROI following perfusion fixation. Next, microCT is exploited to map the EM-processed sample, which identifies the position of the ROI within the resin block (Figure 2C). Although the resin-embedded samples are generally opaque (Box 2), microCT allows imaging of their topology [49,57–60]. The heavy metal stains used during processing for EM generate image contrast in microCT [61,62], revealing the outlines of the resin block, the embedded tissue, and the structural features therein. It was previously demonstrated that microCT imaging reveals DAB-labeled neurons and nano-phosphor particles inside tissue [60]. Importantly, microCT can be further exploited to facilitate and accelerate the correlation between IVM and EM imaging. Endogenous features that are visible in IVM and microCT enable 3D registration of both volumes, accurately determining the position of the ROI inside the EM-processed sample. Subsequently, the resin block can be trimmed quickly and precisely to expose the ROI for 3DEM [49] (Figure 2C and Box 4). Moreover, the registration of the IVM volume to the microCT compensates for the tissue shrinkage introduced by the EM sample preparation, and thus provides high targeting precision ( $<5 \mu\text{m}$ ).

### Applications of Intravital CLEM in Model Systems

The methods described above have enabled the retrieval of transient and rare events within voluminous, complex samples and have facilitated diverse applications in the fields of neuroscience, development, and cancer biology. In this section we outline some of the main findings provided by intravital CLEM studies in commonly used model systems (Box 1).

#### Neuroscience: Pioneering and Pushing intravital CLEM

Neuroscience has undoubtedly been one of driving forces in the development and application of intravital CLEM. Studying the complex neuronal connectivity matrices requires knowledge about the architecture of axons and dendrites, and the locations and strengths of synapses [63]. Using novel tools and probes, FM visualizes some of these features, but only EM reveals the neurons at high resolution in their structural context. Combining functional and long-term IVM imaging with EM thus makes intravital CLEM both popular and instrumental in neurobiological studies. One commonly used model system is the mouse brain, where IVM is performed through a cranial window to image fluorescently labeled neurons in the cortex. Alternatively, *Xenopus* tadpoles [23] and *Drosophila* [19] have been used in intravital CLEM studies to follow synapse formation during neuronal development. In addition to IVM of fluorescent proteins expressed in neurons, neuronal activity can be visualized by calcium imaging (Figure 3A). The preferred response of pyramidal neurons to stimuli of specific orientations was determined by presenting differently angled black and white lines to anesthetized mice, and visualizing the calcium response in a subset of neurons from the visual cortex. Through intravital CLEM, serial section EM revealed that the connectivity between these pyramidal neurons and inhibitory interneurons was dependent on their physical proximity and not on the preferred orientation [64]. When exploring neuronal connectivity and plasticity, EM was often employed as a confirmation or extension of *in vivo* imaging. EM of a small subset of the IVM imaged neurites validates *in vivo* measurements, such as the correlation between fluorescence intensity and the volume of spines [44], boutons [51], or of postsynaptic densities [53]. Importantly, intravital CLEM demonstrated that the shape of spines cannot always be accurately defined by relying solely on resolution-limited IVM [54]. In a series of studies on neural circuit plasticity, the dynamics of spines [42,44] or boutons [24] were monitored over days and months, and the presence of synapses was confirmed by EM. Aiming to define the structural basis of age-induced cognitive decline, EM was also employed to visualize synapses on small spines [50] and large boutons [51] in brains of aged mice. Two studies, mainly relying on intravital CLEM to assess the mechanics of circuit development, demonstrated the unique power of correlative imaging to link ultrastructure to *a priori* knowledge of growth dynamics [21,23]. The age and persistence of spines were analyzed by *in vivo* imaging over a period of  $> 28$  days, and these findings were correlated to the presence of synapses, to spine volume and surface area, and to the neurite connectivity pattern as assessed with EM.



Trends in Cell Biology

**Figure 3. Examples of Intravital CLEM Applications.** (A) *In vivo* two-photon calcium imaging correlated to EM was used to elucidate neuronal networks in the mouse primary visual cortex [64]. (B) Time-lapse IVM of labeled neurons allowed axonal branching dynamics to be studied. Coexpression of GFP and HRP allows the neuron of interest to be retrieved. Once reconstructed using serial TEM (vEM), the postsynaptic profiles from a stable axonal branch are documented [23]. (C) In the zebrafish embryo, intravital CLEM was used to precisely determine the ultrastructure of the endothelial cilia in the blood flow [38]. Abbreviations: HRP, horseradish peroxidase; IVM, intravital microscopy; 2PM, two-photon excitation microscopy; TEM, transmission electron microscopy; vEM, volume electron microscopy; sET, serial electron tomography; 1PM, single-photon excitation microscopy.

Such detailed analysis contradicted the Peters–Miller model of synapse formation and led to the conclusion that a growing spine can form a synapse *de novo*, preferentially with presynaptic elements that are already connected to another spine [21]. Similarly, *in vivo* dendritic branch dynamics in tectal neurons of *Xenopus* tadpoles have been correlated to the distribution, connectivity, and maturity of synapses, as revealed by EM (Figure 3B) [23]. Dynamic dendrites harbor a higher number of synapses compared to stable or retracting ones. During development, branches form multiple synapses, which are then reduced upon stabilization [23].

In summary, intravital CLEM can provide unique insights by combining functional imaging of neurons, via for example *in vivo* calcium imaging, to their detailed structural organization, as visualized by 3DEM. Moreover, long-term monitoring of the development and behavior of

neuronal connections by IVM can be followed by revealing the ultrastructure of the synapses and mapping neuronal organization.

#### Intravital CLEM in Developmental Biology

Intravital CLEM enables the visualization of the ultrastructure of transient processes during development in living model systems, such as mice [22,65], *C. elegans* [17,31], and zebrafish [32,37–40] (Figure 2A). IVM is used to monitor developmental processes, for instance, organogenesis in zebrafish embryo (Figure 2A) [32]. In this work, IVM revealed that the deposition and formation of mechanosensory organs by a migrating primordium is regulated by fibroblast growth factor, which accumulates in a microlumen in the center of the organs. By combining IVM with serial section TEM, it was shown that the microlumen is a well-defined apical space that is contacted by all cells in the organ progenitor [32]. Intravital CLEM in developing zebrafish embryos revealed that the inner structure of endothelial cilia could support their mechanical properties, and thus enable their function as optimal blood-flow sensors. Using serial electron tomography of cilia deflected by the blood flow, it was shown that microtubule content decreases along the axoneme, which potentially regulates their flexural rigidity [38] (Figure 3C). IVM can furthermore be used to pinpoint cells of interest, such as in a recent study of hematopoietic stem and progenitor cells in the caudal hematopoietic tissue niche in zebrafish embryo vasculature. The microenvironment of the lodged cells was imaged by serial section TEM, revealing the contact between hematopoietic stem cells and perivascular niche cells via wrapping, extension of protrusions, or cell–cell attachment [40].

Overall, the application intravital CLEM to embryo models available in developmental biology has the potential to answer unsolved questions related to stem cell origin and fate. As a stand-alone technique, IVM allows the monitoring of developmental processes over time in living organisms, but lacks in resolution the ability to visualize subcellular detail. EM, by contrast, images the sample at high resolution but does not allow rapid screening of crucial developmental events in space and time. For this reason, intravital CLEM is the only technique suitable for studying developmental processes at subcellular resolution. For example, intravital CLEM could help to address the mechanisms of vessel anastomosis [66] or endothelial–hematopoietic transition [67], where the ultrastructural architecture of the cells can be visualized with EM at different steps during the process, as monitored via IVM. In addition, new fast-imaging technologies where low phototoxicity can be exploited to assess developmental events over long periods of time, such as light-sheet microscopy (Box 1), could also be employed. Combining these imaging approaches with high-resolution EM will undoubtedly lead to a better understanding of developmental events.

#### Intravital CLEM in Cancer Biology

Intravital CLEM bears great potential in addressing animal models of human pathologies at a subcellular level. Cancer biology has often been studied by IVM [68], resulting in seminal findings on key aspects of tumor cell invasion or metastasis [69–73]. Recent developments in intravital CLEM captured invasive tumor cells in mouse skin tissue [36]. In this study subcutaneous tumor xenografting in the ear was followed by non-invasive IVM, and subsequent EM. This approach revealed subcellular features of tumor invasion, such as tumor cell protrusions, interaction between tumor cells and the surrounding extracellular matrix, as well a detailed morphology of the invading cells. MicroCT-guided CLEM in the mouse ear significantly reduced the time required to retrieve tiny invasive tumor cells at high resolution, and will undoubtedly lead to new observations that will be instrumental for describing the molecular machineries involved in tumor cell invasion [49]. In particular, this method can provide ultrastructural features of the plasticity of invasive tumor cells and of their microenvironment at the stromal boundary of a tumor xenograft. Furthermore, intravital CLEM was used to track single metastasizing cells in the mouse brain vasculature and to provide, using FIB-SEM (Box 4), details of the early steps of extravasation [49]

(Figure 2C). This study proves that a rare event such as tumor cell extravasation can be assessed at high resolution, *in vivo* in its metastatic niche.

Rare and transient metastatic events, such as invasion, intra- and extravasation, can only be found in living tissue using IVM. IVM can be exploited to not only pinpoint the time and place of the event but also to track the behavior of the tumor cells over time. However, the resolution of IVM is insufficient to reveal the detailed architecture of the tumor cells and does not show their interaction with the microenvironment, which can only be revealed by EM. For instance, only EM can visualize the complexity of the cytoskeletal arrangement, the variety of intracellular organelles that are key elements for cell signaling, and the nature of the cell–cell and cell–extracellular matrix interactions. Intravital CLEM thus provides unique insights into metastatic processes and, in the future, could reveal other features of tumor cell invasion such as extracellular vesicle shedding and uptake [1], tumor/stroma crosstalk, or nuclear squeezing that leads to the rupture of the nuclear envelope [74].

### Concluding Remarks and Future Directions

Combining IVM and EM generates unique insights into the mechanism and architecture of an event of interest taking place inside a living organism. Recently, technological developments, new probes, and improved workflows have made routine, widespread use of intravital CLEM within reach. Most notably in neuroscience, intravital CLEM is used in numerous studies to support IVM observations or as the main method to study neuronal growth dynamics. However, intravital CLEM still requires experience, dedication, time, and, often, sophisticated equipment, which can be challenging for many laboratories. Our own experience proved that tight collaboration between interdisciplinary teams is a rewarding way to circumvent such limitations.

A widespread and routine use of intravital CLEM relies on the development of automated procedures. Automating a multi-step, multi-equipment, and complex procedure such as intravital CLEM is currently not within the realm of possibilities, but some crucial steps can certainly be improved or simplified (see Outstanding Questions). Starting with IVM, much can be gained by improving the spatial resolution and image quality. Super-resolution microscopy (SRM) defies the diffraction limit of light and obtains an *xy* resolution of 10–130 nm [75]. Intravital SRM was previously performed on *C. elegans* [76,77], zebrafish embryos [77,78], and mouse brain [79–81]. The effective resolution of such SRM approaches, however, is hindered by the scattering effect of the tissue. This, in turn, can be compensated for *in vivo* by adjusting an objective correction ring, by wave-front sensing, and adaptive optics aberration correction [82–84]. However, *in vivo* imaging demands high temporal resolution, and some SRM techniques or adaptive optics may currently be too slow to capture transient events. The need for reduced phototoxicity in conjunction with increased temporal resolution is being filled by recent developments in light-sheet microscopy, which opens new avenues for performing long-lasting time-lapse imaging at high resolution [85–87].

IVM could generate additional functional information by making use of different probes, such as fluorescent timers [88,89] and opto-reporters [90]. Moreover, cellular processes can be influenced by photo-activatable genes, which have been used to study synaptic vesicle dynamics in *C. elegans* with EM [91,92]. Following stimulation of light-activated sodium channels, the worm was rapidly (within 20 ms) cryo-immobilized by high-pressure freezing and subsequently processed and imaged with EM [91,92]. In addition, recent developments in fluorescence and chemical biology open the field to the study of nm-sized objects such as nanoparticles within living animals. When combined with EM, such analysis allows the targeting of nanoparticles and analysis of their ultrastructural context [93].

### Outstanding Questions

How can IVM become fully non-invasive to prevent interfering with or disrupting the biological model system?

Can intravital CLEM be performed on spontaneous mouse cancer models and provide understanding of the metastasis cascade?

Can we further enhance the spatial and temporal resolution of IVM? Can we exploit endogenous fluorescence and additional probes to reveal more of the environment of the ROI to facilitate correlation?

How can we introduce cryo-fixation in the intravital CLEM workflow? Following IVM, stabilizing the sample using cryo-fixation will arrest the event of interest as it takes place. Moreover, cryo-fixation not only improves the ultrastructural preservation of the sample but also would be an obligatory step for developing cryo-CLEM.

How can image processing and data analysis be automated? Will it be possible to fully automate segmentation and annotation of the cell ultrastructure?

How can the throughput of the correlative workflow be increased to study large numbers of samples?

Will CLEM become a routine approach, comparable to confocal microscopy, which is accessible for all scientists?

Correlating IVM to EM is easiest when datasets from both modalities largely overlap: this enables the identification of a larger number of common landmarks, which improves the registration of the imaged volumes. IVM typically provides a large field of view, but volume imaging by TEM required large numbers of serial sections. A TEM camera array employed in an intravital CLEM study extended the field of view of EM [64]. Similarly, a multi-SEM was developed that combines > 61 electron beams and detectors [94]. Importantly, a number of recent developments have resulted in automated volume EM (see Table 1 in Box 3). With FIB-SEM and SEM, an interplay between dedicated hardware and software enables sectioning and imaging with limited assistance of an operator. Automated serial imaging in SEM has the potential to bridge the need for large volume acquisition when correlating EM to LM. The use of these techniques in CLEM is expected to dramatically increase in the near future.

Finally, the ease-of-use and throughput of intravital CLEM could be significantly improved by automating the retrieval of the ROI and the analysis of the data. In intravital CLEM, correlating the different datasets is primarily performed manually using commercially available software, such as Adobe Photoshop [32,36,38] or Amira [20,36,49], but also using freeware such as Fiji [40,64,95] and potentially Icy [96]. However, no software is currently available that enables fully automatic alignment between 2D or 3D IVM and EM volumes. Following EM imaging of the ROI, the stack of EM images that make up the 3D volume need to be aligned, mostly performed with TrakEM (Fiji) [36,41,48–54,97] and the structure of interest may be highlighted by segmentation. Segmentation enables 3D visualization of the ROI and can be crucial for correlation between IVM and EM [54]. To automate segmentation, machine-learning software is being developed and constantly improved [98,99]. However, the majority of segmentation work on EM volumes still involves time-consuming manual labor.

In conclusion, intravital CLEM is a developing field that could gain accessibility by simplifying and automating crucial workflow steps. Because intravital CLEM combines IVM and EM, the potential of the approach is restricted by the limitations of both techniques. Then again, the developments recently achieved for both IVM and EM contribute to intravital CLEM as a whole. Further improvements, especially in dedicated registration and image-processing software, will enhance the throughput of intravital CLEM, allowing quantitative structure–function studies to be performed *in vivo*.

### Acknowledgments

M.A.K. is supported by an EMBL Interdisciplinary Postdoctoral fellowship (EIPOD) under Marie Curie Actions (COFUND). V. H. receives support from the French National Cancer Institute (INCa). Y.S. receives grant support from the EMBL. Research in the laboratory of J.G.G. is supported by funding from University of Strasbourg, Investissements d'Avenir (IdEx), the INSERM, the French National Cancer Institute (INCa), the Canceropole Grand-Est, the Plan Cancer, the Ligue contre le Cancer, and ROCHE.

### References

- Zomer, A. *et al.* (2015) *In vivo* imaging reveals extracellular vesicle-mediated phenocopying of metastatic behavior. *Cell* 161, 1046–1057
- Erami, Z. *et al.* (2016) Intravital FRAP imaging using an E-cadherin–GFP mouse reveals disease- and drug-dependent dynamic regulation of cell–cell junctions in live tissue. *Cell Rep.* 14, 152–167
- Chèvre, R. *et al.* (2014) High-resolution imaging of intravascular atherogenic inflammation in live mice. *Circ. Res.* 114, 770–779
- Lämmermann, T. *et al.* (2013) Neutrophil swarms require LTB4 and integrins at sites of cell death *in vivo*. *Nature* 498, 371–375
- Al Jord, A. *et al.* (2014) Centriole amplification by mother and daughter centrioles differs in multiciliated cells. *Nature* 516, 104–107
- Avinoam, O. *et al.* (2015) Endocytic sites mature by continuous bending and remodeling of the clathrin coat. *Science* 348, 1369–1372
- Briggman, K.L. *et al.* (2011) Wiring specificity in the direction-selectivity circuit of the retina. *Nature* 471, 183–188
- Kukulski, W. *et al.* (2012) Plasma membrane reshaping during endocytosis is revealed by time-resolved electron tomography. *Cell* 150, 508–520
- Van Engelenburg, S.B. *et al.* (2014) Distribution of ESCRT machinery at HIV assembly sites reveals virus scaffolding of ESCRT subunits. *Science* 343, 653–656
- Meisslitzer-Ruppitsch, C. *et al.* (2009) Photooxidation technology for correlated light and electron microscopy. *J. Microsc.* 235, 322–335

11. Caplan, J. *et al.* (2011) The power of correlative microscopy: multi-modal, multi-scale, multi-dimensional. *Curr. Opin. Struct. Biol.* 21, 686–693
12. Mironov, A.A. and Beznoussenko, G.V. (2009) Correlative microscopy: a potent tool for the study of rare or unique cellular and tissue events. *J. Microsc.* 235, 308–321
13. de Boer, P. *et al.* (2015) Correlated light and electron microscopy: ultrastructure lights up! *Nat. Methods* 12, 503–513
14. Loussert Fonta, C. and Humbel, B.M. (2015) Correlative microscopy. *Arch. Biochem. Biophys.* 581, 98–110
15. Müller-Reichert, T. and Verkade, P., eds (2012) *Correlative Light and Electron Microscopy*, Academic Press
16. Müller-Reichert, T. and Verkade, P., eds (2014) In *Correlative Light and Electron Microscopy*. (2), Academic Press
17. Müller-Reichert, T. *et al.* (2007) Correlative light and electron microscopy of early *Caenorhabditis elegans* embryos in mitosis. *Methods Cell Biol.* 79, 101–119
18. Sims, P.A. and Hardin, J.D. (2007) Fluorescence-integrated transmission electron microscopy images: integrating fluorescence microscopy with transmission electron microscopy. *Methods Mol. Biol.* 369, 291–308
19. Zito, K. *et al.* (1999) Watching a synapse grow: noninvasive confocal imaging of synaptic growth in *Drosophila*. *Neuron* 22, 719–729
20. Hosseini, R. *et al.* (2014) Correlative light and electron microscopy imaging of autophagy in a zebrafish infection model. *Autophagy* 10, 1844–1857
21. Knott, G.W. *et al.* (2006) Spine growth precedes synapse formation in the adult neocortex in vivo. *Nat. Neurosci.* 9, 1117–1124
22. Sandoval, R.M. (2004) Uptake and trafficking of fluorescent conjugates of folic acid in intact kidney determined using intravital two-photon microscopy. *AJP: Cell Physiol.* 287, C517–C526
23. Li, J. *et al.* (2011) In vivo time-lapse imaging and serial section electron microscopy reveal developmental synaptic rearrangements. *Neuron* 69, 273–286
24. De Paola, V. *et al.* (2006) Cell type-specific structural plasticity of axonal branches and boutons in the adult neocortex. *Neuron* 49, 861–875
25. Gan, W.B. *et al.* (1999) Vital imaging and ultrastructural analysis of individual axon terminals labeled by iontophoretic application of lipophilic dye. *J. Neurosci. Methods* 93, 13–20
26. Gaietta, G. *et al.* (2002) Multicolor and electron microscopic imaging of connexin trafficking. *Science* 296, 1–5
27. Luby-Phelps, K. *et al.* (2003) Visualization of identified GFP-expressing cells by light and electron microscopy. *J. Histochem. Cytochem.* 51, 271–274
28. Watanabe, S. *et al.* (2011) Protein localization in electron micrographs using fluorescence nanoscopy. *Nat. Methods* 8, 80–84
29. Nixon, S.J. *et al.* (2009) A single method for cryofixation and correlative light, electron microscopy and tomography of zebrafish embryos. *Traffic* 10, 131–136
30. Kukulski, W. *et al.* (2011) Correlated fluorescence and 3D electron microscopy with high sensitivity and spatial precision. *J. Cell Biol.* 192, 111–119
31. Kolotuev, I. *et al.* (2010) A precise and rapid mapping protocol for correlative light and electron microscopy of small invertebrate organisms. *Biol. Cell* 102, 121–132
32. Durdu, S. *et al.* (2014) Luminal signalling links cell communication to tissue architecture during organogenesis. *Nature* 515, 120–124
33. Kamoun, W.S. *et al.* (2008) Liver microcirculation analysis by red blood cell motion modeling in intravital microscopy images. *IEEE Trans. Biomed. Eng.* 55, 162–170
34. Beacham, W.S. *et al.* (1976) Observations of the microcirculatory bed in rat mesoecum using differential interference contrast microscopy in vivo and electron microscopy. *Am. J. Anat.* 146, 385–425
35. Fox, J. *et al.* (1980) Action of histamine on the mesenteric microvasculature. *Microvasc. Res.* 19, 108–126
36. Karreman, M.A. *et al.* (2014) Correlating intravital multi-photon microscopy to 3D electron microscopy of invading tumor cells using anatomical reference points. *PLoS ONE* 9, e114448
37. Armer, H.E.J. *et al.* (2009) Imaging transient blood vessel fusion events in zebrafish by correlative volume electron microscopy. *PLoS ONE* 4, e7716
38. Goetz, J.G. *et al.* (2014) Endothelial cilia mediate low flow sensing during zebrafish vascular development. *Cell Rep.* 6, 799–808
39. van Ham, T.J. *et al.* (2014) Intravital correlated microscopy reveals differential macrophage and microglial dynamics during resolution of neuroinflammation. *Dis. Model. Mech.* 7, 857–869
40. Tamplin, O.J. *et al.* (2015) Hematopoietic stem cell arrival triggers dynamic remodeling of the perivascular niche. *Cell* 160, 241–252
41. Li, J. *et al.* (2010) Membrane targeted horseradish peroxidase as a marker for correlative fluorescence and electron microscopy studies. *Front. Neural Circuits* 4, 1–10
42. Trachtenberg, J.T. *et al.* (2002) Long-term in vivo imaging of experience-dependent synaptic plasticity in adult cortex. *Nature* 420, 788–794
43. Holtmaat, A.J.G.D. *et al.* (2005) Transient and persistent dendritic spines in the neocortex in vivo. *Neuron* 45, 279–291
44. Holtmaat, A. *et al.* (2006) Experience-dependent and cell-type-specific spine growth in the neocortex. *Nature* 441, 979–983
45. Knott, G.W. *et al.* (2009) A protocol for preparing GFP-labeled neurons previously imaged in vivo and in slice preparations for light and electron microscopic analysis. *Nat. Protoc.* 4, 1145–1156
46. Dunaevsky, A. *et al.* (2001) Spine motility with synaptic contact. *Nat. Neurosci.* 4, 685–686
47. Bishop, D. *et al.* (2011) Near-infrared branding efficiently correlates light and electron microscopy. *Nat. Methods* 8, 568–570
48. Maco, B. *et al.* (2013) Correlative in vivo 2-photon and focused ion beam scanning electron microscopy of cortical neurons. *PLoS ONE* 8, e57405
49. Karreman, M.A. *et al.* (2016) Fast and precise targeting of single tumor cells in vivo by multimodal correlative microscopy. *J. Cell Sci.* 129, 444–456
50. Mostany, R. *et al.* (2013) Altered synaptic dynamics during normal brain aging. *J. Neurosci.* 33, 4094–4104
51. Grillo, F.W. *et al.* (2013) Increased axonal bouton dynamics in the aging mouse cortex. *PNAS* 110, E1514–E1523
52. Canty, A.J. *et al.* (2013) In-vivo single neuron axotomy triggers axon regeneration to restore synaptic density in specific cortical circuits. *Nat. Commun.* 4, 2038
53. Cane, M. *et al.* (2014) The relationship between PSD-95 clustering and spine stability in vivo. *J. Neurosci.* 34, 2075–2086
54. Blazquez-Llorca, L. *et al.* (2015) Correlation of two-photon in vivo imaging and FIB/SEM microscopy. *J. Microsc.* 259, 129–136
55. Maco, B. *et al.* (2014) Correlative in vivo 2-photon imaging and focused ion beam scanning electron microscopy: 3D analysis of neuronal ultrastructure. In *Methods in Cell Biology: Correlative Microscopy II* (1st edn) (Mueller-Reichert, T. and Verkade, P., eds), pp. 339–361, Elsevier
56. Maco, B. *et al.* (2014) Semiautomated correlative 3D electron microscopy of in vivo-imaged axons and dendrites. *Nat. Protoc.* 9, 1354–1366
57. Handschuh, S. *et al.* (2013) A correlative approach for combining microCT, light and transmission electron microscopy in a single 3D scenario. *Front. Zool.* 10, 1–16
58. Sengle, G. *et al.* (2013) A correlative method for imaging identical regions of samples by micro-CT, light microscopy, and electron microscopy: imaging adipose tissue in a model system. *J. Histochem. Cytochem.* 61, 263–271
59. Keene, D.R. *et al.* (2014) Correlation of the same fields imaged in the TEM, confocal, LM, and microCT by image registration: from specimen preparation to displaying a final composite image. In *Methods in Cell Biology: Correlative Microscopy II* (1st edn) (Mueller-Reichert, T. and Verkade, P., eds), pp. 391–417, Elsevier
60. Bushong, E.A. *et al.* (2014) X-ray microscopy as an approach to increasing accuracy and efficiency of serial block-face imaging for correlated light and electron microscopy of biological specimens. *Microsc. Microanal.* 21, 231–238
61. Johnson, J.T. *et al.* (2006) Virtual histology of transgenic mouse embryos for high-throughput phenotyping. *PLoS Genet.* 2, e61

62. Metscher, B.D. (2009) MicroCT for comparative morphology: simple staining methods allow high-contrast 3D imaging of diverse non-mineralized animal tissues. *BMC Physiol.* 9, 11
63. Helmstaedter, M. *et al.* (2008) 3D structural imaging of the brain with photons and electrons. *Curr. Opin. Neurobiol.* 18, 633–641
64. Bock, D.D. *et al.* (2012) Network anatomy and in vivo physiology of visual cortical neurons. *Nature* 471, 177–182
65. Lomonte, B. *et al.* (1994) The dynamics of local tissue damage induced by *Bothrops asper* snake venom and myotoxin II on the mouse cremaster muscle: an intravital and electron microscopic study. *Toxicol.* 32, 41–55
66. Lenard, A. *et al.* (2013) In vivo analysis reveals a highly stereotypic morphogenetic pathway of vascular anastomosis. *Dev. Cell* 25, 492–506
67. Kissa, K. and Herbomel, P. (2010) Blood stem cells emerge from aortic endothelium by a novel type of cell transition. *Nature* 464, 112–115
68. Ellenbroek, S.I.J. and van Rheenen, J. (2014) Imaging hallmarks of cancer in living mice. *Nat. Rev. Cancer* 14, 406–418
69. Hirata, E. *et al.* (2015) Intravital imaging reveals how BRAF inhibition generates drug-tolerant microenvironments with high integrin  $\beta$ 1/FAK signaling. *Cancer Cell* 27, 574–588
70. Alexander, S. *et al.* (2013) Preclinical intravital microscopy of the tumour–stroma interface: invasion, metastasis, and therapy response. *Curr. Opin. Cell Biol.* 25, 659–671
71. Kienast, Y. *et al.* (2010) Realtime imaging reveals the single steps of brain metastasis formation. *Nat. Med.* 16, 116–122
72. Provenzano, P.P. *et al.* (2012) Enzymatic targeting of the stroma ablates physical barriers to treatment of pancreatic ductal adenocarcinoma. *Cancer Cell* 21, 418–429
73. Lohela, M. *et al.* (2014) Intravital imaging reveals distinct responses of depleting dynamic tumor-associated macrophage and dendritic cell subpopulations. *PNAS* 111, E5086–E5095
74. Denais, C.M. *et al.* (2016) Nuclear envelope rupture and repair during cancer cell migration. *Science* 352, 353–358
75. Sydor, A.M. *et al.* (2015) Super-resolution microscopy: from single molecules to supramolecular assemblies. *Trends Cell Biol.* 25, 730–748
76. Rankin, B.R. *et al.* (2011) Nanoscopy in a living multicellular organism expressing GFP. *Biophys. J.* 100, L63–L65
77. York, A.G. *et al.* (2012) Resolution doubling in live, multicellular organisms via multifocal structured illumination microscopy. *Nat. Methods* 9, 749–754
78. Gabor, K.A. *et al.* (2015) Nanoscale imaging of caveolin-1 membrane domains in vivo. *PLoS ONE* 10, e0117225
79. Berning, S. *et al.* (2012) Nanoscopy in a living mouse brain. *Science* 335, 551
80. Willig, K.I. *et al.* (2014) Nanoscopy of filamentous actin in cortical dendrites of a living mouse. *Biophys. J.* 106, L01–L03
81. Agarwal, A. *et al.* (2014) Dysregulated expression of neuregulin-1 by cortical pyramidal neurons disrupts synaptic plasticity. *Cell Rep.* 8, 1130–1145
82. Gould, T.J. *et al.* (2012) Adaptive optics enables 3D STED microscopy in aberrating specimens. *Opt. Express* 20, 20998–21009
83. Hell, S.W. *et al.* (2015) The 2015 super-resolution microscopy roadmap. *J. Phys. D: Appl. Phys.* 48, 443001–443036
84. Wang, K. *et al.* (2015) Direct wavefront sensing for high-resolution in vivo imaging in scattering tissue. *Nat. Commun.* 6, 1–6
85. Chhetri, R.K. *et al.* (2015) Whole-animal functional and developmental imaging with isotropic spatial resolution. *Nat. Methods* 12, 1171–1178
86. Strnad, P. *et al.* (2015) Inverted light-sheet microscope for imaging mouse pre-implantation development. *Nat. Methods* 13, 139–142
87. Reynaud, E.G. *et al.* (2015) Guide to light-sheet microscopy for adventurous biologists. *Nat. Methods* 12, 30–34
88. Terskikh, A. *et al.* (2000) “Fluorescent timer”: protein that changes color with time. *Science* 290, 1585–1588
89. Butko, M.T. *et al.* (2012) Fluorescent and photo-oxidizing Time-STAMP tags track protein fates in light and electron microscopy. *Nat. Neurosci.* 15, 1742–1751
90. Alford, S.C. *et al.* (2012) Optogenetic reporters. *Biol. Cell* 105, 14–29
91. Watanabe, S. *et al.* (2014) Flash-and-freeze electron microscopy: coupling optogenetics with high-pressure freezing. In *Nanoscale Imaging of Synapses: New Concepts and Opportunities*, (Nägerl, U.V. and Triller, A., eds), pp. 43–56, Springer Science+Business Media
92. Watanabe, S. *et al.* (2013) Ultrafast endocytosis at *Caenorhabditis elegans* neuromuscular junctions. *eLife* 2, e00723
93. Wolfbeis, O.S. (2015) An overview of nanoparticles commonly used in fluorescent bioimaging. *Chem. Soc. Rev.* 44, 4743–4768
94. Eberle, A.L. *et al.* (2015) High-resolution, high-throughput imaging with a multibeam scanning electron microscope. *J. Microsc.* 259, 114–120
95. Schindelin, J. *et al.* (2012) Fiji: an open-source platform for biological-image analysis. *Nat. Methods* 9, 676–682
96. de Chaumont, F. *et al.* (2012) Icy: an open bioimage informatics platform for extended reproducible research. *Nat. Methods* 9, 690–696
97. Allegra Mascaro, A.L. *et al.* (2013) In vivo single branch axotomy induces GAP-43-dependent sprouting and synaptic remodeling in cerebellar cortex. *PNAS* 110, 10824–10829
98. Sommer, C. *et al.* (2011) ilastik: Interactive learning and segmentation toolkit. In *Proceedings of the 8th IEEE International Symposium on Biomedical Imaging*, 230–233
99. Belevich, I. *et al.* (2016) Microscopy image browser: a platform for segmentation and analysis of multidimensional datasets. *PLoS Biol.* 14, e1002340
100. White, R. *et al.* (2013) Zebrafish cancer: the state of the art and the path forward. *Nat. Rev. Cancer* 13, 624–636
101. Kaufman, C.K. *et al.* (2016) A zebrafish melanoma model reveals emergence of neural crest identity during melanoma initiation. *Science* 351, 1–10
102. Mickoleit, M. *et al.* (2014) High-resolution reconstruction of the beating zebrafish heart. *Nat. Methods* 11, 919–922
103. Li, J.L. *et al.* (2012) Intravital multiphoton imaging of immune responses in the mouse ear skin. *Nat. Protoc.* 7, 221–234
104. Mercier, L. *et al.* (2016) In vivo imaging of skeletal muscle in mice highlights muscle defects in a mouse model of myotubular myopathy. *IntraVital* 0, 1–12
105. Headley, M.B. *et al.* (2016) Visualization of immediate immune responses to pioneer metastatic cells in the lung. *Nature* 531, 513–517
106. Ritsma, L. *et al.* (2012) Intravital microscopy through an abdominal imaging window reveals a pre-micrometastasis stage during liver metastasis. *Sci. Trans. Med.* 4, 1–11
107. Alexander, S. *et al.* (2008) Dynamic imaging of cancer growth and invasion: a modified skin-fold chamber model. *Histochem. Cell Biol.* 130, 1147–1154
108. Choi, M. *et al.* (2015) In vivo fluorescence microscopy: lessons from observing cell behavior in their native environment. *Physiology* 30, 40–49
109. Keikhosravi, A. *et al.* (2014) Second-harmonic generation imaging of cancer. In *Methods in Cell Biology: Quantitative Imaging in Cell Biology*, (Waters, J.C. and Wittman, T., eds), pp. 531–546, Elsevier Masson SAS
110. Weigel, B. *et al.* (2016) Third harmonic generation microscopy of cells and tissue organization. *J. Cell Sci.* 129, 245–255
111. Daemen, S. *et al.* (2016) Microscopy tools for the investigation of intracellular lipid storage and dynamics. *Mol. Metab.* 5, 153–163
112. Follain, G. *et al.* (2016) Seeing is believing: multi-scale spatio-temporal imaging towards in vivo cell biology. *J. Cell Sci.* <http://dx.doi.org/10.1242/jcs.189001>
113. Korogod, N. *et al.* (2015) Ultrastructural analysis of adult mouse neocortex comparing aldehyde perfusion with cryo fixation. *eLife* 4, e05793
114. Humbel, B.M. and Müller, M. (1985) Freeze substitution and low temperature embedding. In *Science of Biological Specimen Preparation*, (Müller, M. *et al.*, eds), pp. 175–183, SEM Inc., AMF O'Hare
115. Dubochet, J. (1995) High-pressure freezing for cryoelectron microscopy. *Trends Cell Biol.* 5, 366–368

116. Harapin, J. *et al.* (2015) Structural analysis of multicellular organisms with cryo-electron tomography. *Nat. Methods* 12, 634–636
117. Shu, X. *et al.* (2011) A genetically encoded tag for correlated light and electron microscopy of intact cells, tissues, and organisms. *PLoS Biol.* 9, e1001041
118. Kuipers, J. *et al.* (2015) FLIPPER, a combinatorial probe for correlated live imaging and electron microscopy, allows identification and quantitative analysis of various cells and organelles. *Cell Tissue Res.* 360, 61–70
119. Ariotti, N. *et al.* (2015) Modular detection of GFP-labeled proteins for rapid screening by electron microscopy in cells and organisms. *Dev. Cell* 35, 1–14
120. Lam, S.S. *et al.* (2015) Directed evolution of APEX2 for electron microscopy and proximity labeling. *Nat. Methods* 12, 51–54
121. Ngo, J.T. *et al.* (2016) Click-EM for imaging metabolically tagged nonprotein biomolecules. *Nat. Chem. Biol.* 12, 459–465
122. Gaietta, G. (2002) Multicolor and electron microscopic imaging of connexin trafficking. *Science* 296, 503–507
123. Han, H.-S. *et al.* (2015) Quantum dot/antibody conjugates for in vivo cytometric imaging in mice. *PNAS* 112, 1350–1355
124. Birch-Andersen, A. (1955) Reconstruction of the nuclear sites of *Salmonella typhimurium* from electron micrographs of serial sections. *J. Gen. Microbiol.* 13, 327–329
125. Harris, K.M. *et al.* (2006) Uniform serial sectioning for transmission electron microscopy. *J. Neurosci.* 26, 12101–12103
126. Hohmann-Marriott, M.F. *et al.* (2009) Nanoscale 3D cellular imaging by axial scanning transmission electron tomography. *Nat. Methods* 6, 729–731
127. Biskupek, J. *et al.* (2010) Optimization of STEM tomography acquisition—a comparison of convergent beam and parallel beam STEM tomography. *Ultramicroscopy* 110, 1231–1237
128. Briggman, K.L. and Bock, D.D. (2012) Volume electron microscopy for neuronal circuit reconstruction. *Curr. Opin. Neurobiol.* 22, 154–161
129. Wacker, I. and Schroeder, R.R. (2013) Array tomography. *J. Microsc.* 252, 93–99
130. Peddie, C.J. and Collinson, L.M. (2014) Exploring the third dimension: volume electron microscopy comes of age. *Micron* 61, 9–19
131. Miranda, K. *et al.* (2015) Three dimensional reconstruction by electron microscopy in the life sciences: an introduction for cell and tissue biologists. *Mol. Reprod. Dev.* 82, 530–547
132. Eberle, A.L. *et al.* (2015) Mission (im)possible—mapping the brain becomes a reality. *Microscopy* 64, 45–55
133. Micheva, K.D. and Smith, S.J. (2007) Array tomography: a new tool for imaging the molecular architecture and ultrastructure of neural circuits. *Neuron* 55, 25–36
134. Oberti, D. *et al.* (2010) Correlative microscopy of densely labeled projection neurons using neural tracers. *Front. Neuroanat.* 4, 1–7
135. Oberti, D. *et al.* (2011) Projection neuron circuits resolved using correlative array tomography. *Front. Neurosci.* 5, 1–8
136. Collman, F. *et al.* (2015) Mapping synapses by conjugate light-electron array tomography. *J. Neurosci.* 35, 5792–5807
137. Horstmann, H. *et al.* (2012) Serial section scanning electron microscopy (SSEM) on silicon wafers for ultra-structural volume imaging of cells and tissues. *PLoS ONE* 7, e35172
138. Reichelt, M. *et al.* (2012) 3D reconstruction of VZV infected cell nuclei and PML nuclear cages by serial section array scanning electron microscopy and electron tomography. *PLoS Pathog.* 8, e1002740
139. Hayworth, K.J. *et al.* (2006) Automating the collection of ultrathin serial sections for large volume TEM reconstructions. *Microsc. Microanal.* 12, 86–87
140. Schalek, R. *et al.* (2011) Development of high-throughput, high-resolution 3D reconstruction of large-volume biological tissue using automated tape collection ultramicrotomy and scanning electron microscopy. *Microsc. Microanal.* 17, 966–967
141. Hayworth, K.J. *et al.* (2014) Imaging ATUM ultrathin section libraries with WaferMapper: a multi-scale approach to EM reconstruction of neural circuits. *Front. Neural Circuits* 8, 1–18
142. Narayan, K. and Subramaniam, S. (2015) Focused ion beams in biology. *Nat. Methods* 12, 1021–1031
143. Kuzirian, A.M. and Leighton, S.B. (1983) Oxygen plasma etching of entire block face improves the resolution and usefulness of serial scanning electron microscopic images. *Scan. Electron Microsc.* 4, 1877–1885
144. Denk, W. and Horstmann, H. (2004) Serial block-face scanning electron microscopy to reconstruct three-dimensional tissue nanostructure. *PLoS Biol.* 2, e329